Available online at www.sciencedirect.com
SCIENCE DIRECT®
International Journal of Heat and Mass Transfer 47 (2004) 395–406
International Journal of HEAT and MASS TRANSFER
www.elsevier.com/locate/ijhmt

# Simplified models for coupled heat and mass transfer in falling-film absorbers

Md. Raisul Islam, N.E. Wijeysundera *, J.C. Ho

*Department of Mechanical and Production Engineering, National University of Singapore, 10 Kent Ridge Crescent, Singapore 119260, Singapore*

Received 28 October 2002

**Abstract**

A linearized coupled model is developed for the heat and mass transfer in falling-film absorbers. Its accuracy is established by comparing the predictions with those of a non-linear model and a numerical simulation. Under certain conditions, the linearized model reduces to the log-mean-difference formulation. The linearized model yields analytical expressions that are used to determine heat and mass transfer coefficients from the experimental data for a horizontal tubular absorber and a vertical tube absorber. The overall Nusselt number and Sherwood number for the tubular absorber increase with increasing film Reynolds number and inlet cooling water temperature. The cooling water temperature distribution predicted by the linearized model agrees well with measurements.


*Keywords:* Vapor absorption systems; Absorber design; Coupled models; Transfer coefficients; Numerical simulation

## 1. Introduction

The modeling of heat and mass transfer processes in the absorbers of conventional absorption refrigeration systems has received considerable attention in the recent literature. A critical review of the various modeling techniques was presented by Killion and Garimella [1]. There have been a number of efforts to develop coupled models that are suitable for the design of absorbers. Patnaik and Perez-Blanco [2] and Patnaik et al. [3] developed simplified design approaches for absorbers by treating them as counter-flow heat and mass exchangers. Conlisk [4] presented a design procedure for absorbers. Ryan [5] analyzed water absorption in an adiabatic spray of aqueous LiBr solution. Wekken and Wassenaar [6] solved the coupled heat and mass transfer equations for the absorption of vapor in a laminar falling film. Tsai and Perez-Blanco [7] and Andberg and Vliet [8] developed simplified models for falling-film absorbers. Uddholm and Settewall [9] used a model to predict the wave frequencies of the falling film. Choudhury et al. [10] developed a numerical model for vertical film flow. Grossman [11] presented an analytical model for the absorption of vapor in a laminar falling film. Choudhury et al. [10] developed a numerical model for vertical film flow. Grossman [11] presented an analytical model for the absorption of vapor in a laminar falling film. Yüksel and Schlünder [12,13] studied the variation of the heat and mass transfer coefficients in a falling film of aqueous LiBr solution. Their work highlighted the importance of the coupling between the heat and mass transfer processes at the liquid–vapor interface.

Simulations of the heat and mass transfer processes in absorbers have been performed by using physical models of varying complexity [1]. Numerical models in which the conservation equations of mass, momentum and energy are solved simultaneously are the most detailed of these. Formulations that follow traditional heat exchanger analysis require as input the variation of the heat and mass transfer coefficients for the falling film. The analysis of experimental data to determine the heat

* Corresponding author. Tel.: +65-874-2558; fax: +65-779-1459.
*E-mail address:* mpewijey@nus.edu.sg (N.E. Wijeysundera).

0017-9310/$ - see front matter © 2003 Elsevier Ltd. All rights reserved.
doi:10.1016/j.ijheatmasstransfer.2003.07.001

**Nomenclature**

| | |
|---|---|
| $a$ | constant in equilibrium relationship |
| $A$ | absorber area [$m^2$] |
| $A_t$ | total area of absorber [$m^2$] |
| $b$ | coefficient in equilibrium relationship [$K^{-1}$] |
| $C_{pw}$ | specific heat capacity of water [$J\,kg^{-1}\,K^{-1}$] |
| $dm_{ws}$ | change in vapor absorption rate [$kg\,s^{-1}$] |
| $dM_s$ | change in mass flow rate of solution [$kg\,s^{-1}$] |
| $dQ_i$ | heat flow rate from solution to wall [W] |
| $dQ_o$ | heat flow rate from interface to bulk solution [W] |
| $D_{AB}$ | mass diffusivity [$m^2\,s^{-1}$] |
| $g$ | gravitational acceleration [$m\,s^{-2}$] |
| $h_i$ | heat transfer coefficient from bulk solution to wall [$W\,m^{-2}\,K^{-1}$] |
| $h_o$ | heat transfer coefficient from interface to bulk solution [$W\,m^{-2}\,K^{-1}$] |
| $h_w$ | convective heat transfer coefficient for cooling water [$W\,m^{-2}\,K^{-1}$] |
| $i_{ab}$ | enthalpy of absorption [$J\,kg^{-1}$] |
| $i_{pw}$ | partial enthalpy of water at the interface [$J\,kg^{-1}$] |
| $i_s$ | enthalpy of solution [$J\,kg^{-1}$] |
| $i_v$ | enthalpy of water vapor at film interface [$J\,kg^{-1}$] |
| $i_{vs}$ | difference in enthalpy [$J\,kg^{-1}$] |
| $K_{ef}$ | effective mass transfer coefficient from interface to bulk solution [$m\,s^{-1}$] |
| $K_m$ | mass transfer coefficient from interface to bulk solution [$m\,s^{-1}$] |
| $k_s$ | thermal conductivity of solution [$W\,m^{-1}\,K^{-1}$] |
| $k_{wall}$ | thermal conductivity of tube wall [$W\,m^{-1}\,K^{-1}$] |
| $L$ | length of absorber [m] |
| $m_v$ | mass flux of vapor at film interface [$kg\,m^{-2}\,s^{-1}$] |
| $m_{ws}$ | vapor absorption rate in the solution [$kg\,s^{-1}$] |
| $M_{abs}$ | total vapor absorption rate [$kg\,s^{-1}$] |
| $M_l$ | mass flow rate of LiBr [$kg\,s^{-1}$] |
| $M_s$ | mass flow rate of solution [$kg\,s^{-1}$] |
| $M_w$ | mass flow rate of cooling water [$kg\,s^{-1}$] |
| $Nu_i$ | Nusselt number $\frac{h_i\delta}{k_s}$ |
| $Nu_o$ | Nusselt number $\frac{h_o\delta}{k_s}$ |
| $q$ | heat flux at film interface [$W\,m^{-2}$] |
| $Q$ | heat transfer rate [W] |
| $Re$ | Reynolds number $4\,\Gamma/\mu$ |
| $Sh$ | Sherwood number $\frac{K_m\delta}{D_{AB}}$ |
| $T$ | temperature [°C] |
| $U$ | solution velocity in $X$-direction [$m\,s^{-1}$] |
| $U_{bw}$ | overall heat transfer coefficient from bulk solution to coolant [$W\,m^{-2}\,K^{-1}$] |
| $V$ | solution velocity in $Y$-direction [$m\,s^{-1}$] |
| $X$ | coordinate in the direction of solution flow [m] |
| $Y$ | coordinate in the direction of the film thickness [m] |
| $Z$ | coordinate in the direction of film width [m] |

*Greek symbols*

| | |
|---|---|
| $\theta$ | temperature difference between bulk solution and coolant [°C] |
| $\psi$ | difference between bulk solution concentration and equilibrium concentration corresponding to local solution temperature |
| $\delta$ | film thickness [m] |
| $\delta_{wall}$ | wall thickness of absorber plate or tube [m] |
| $\Gamma$ | mass flow rate of solution per unit width of film [$kg\,m^{-1}\,s^{-1}$] |
| $\rho$ | density [$kg\,m^{-3}$] |
| $\omega$ | mass concentration of LiBr |
| $\alpha$ | thermal diffusivity [$m^2\,s^{-1}$] |
| $v$ | kinematic viscosity of solution [$m^2\,s^{-1}$] |

*Subscripts and superscripts*

| | |
|---|---|
| – | average |
| ex | exit of absorber |
| if | solution–vapor interface |
| in | coolant inlet |
| s | solution |
| sb | bulk solution |
| o | entrance of absorber |
| w | water |
| wall | absorber wall |

and mass transfer coefficients has been based on the log-mean-difference (LMD) approach. Several variations of the LMD quantities have been adopted in the literature. Unfortunately, the heat and mass transfer coefficients obtained by these different approaches seldom show agreement [14].

The aim of the present study is to develop a simplified coupled model that could be used to design absorbers and extract heat and mass transfer coefficients from experimental data. The simplified models, however, require a knowledge of the heat and mass transfer coefficients, which for purposes of validation, are obtained from a detailed numerical simulation. Following this approach, it is possible to develop a coupled heat and mass transfer model that yields closed-form expressions for the various parameters of the falling film.

## 2. Simplified models for absorbers

### 2.1. Non-linear coupled model

The counter-flow absorber is represented schematically as shown in Fig. 1. In the first simplified model outlined below, the change in solution mass flow rate due to the absorption of vapor is included. The heat and mass transfer from the vapor–liquid interface of the film to the bulk solution is represented by a heat transfer coefficient $h_o$ and a mass transfer coefficient $K_m$ respectively. The heat transfer coefficients from the bulk solution to the wall and the wall to the coolant are $h_i$ and $h_w$ respectively. $U_{bw}$ is the overall heat transfer coefficient from the bulk solution to the coolant. Grossman [11] studied the variation of these transfer coefficients for a laminar falling film using an analytical model. Similar heat and mass transfer coefficients were defined by Yüksel and Schlünder [12,13] in their experimental and theoretical work. Considering a small control volume the mass conservation equation for the solution can be written as

$$(M_s + dM_s) = dm_{ws} + M_s \tag{1}$$

where the first term on the RHS is the vapor absorption rate.

Following the derivation of Tsai and Perez-Blanco [7], the energy conservation equation for the control volume at steady-state can be expressed as

$$M_s i_s + i_v dm_{ws} = (M_s + dM_s)(i_s + di_s) + U_{bw}(T_{sb} - T_w)\,dA \tag{2}$$

where $i_s$ is the enthalpy of the solution and $i_v$ is the enthalpy of the vapor. The second term on the RHS of Eq. (2) is the heat transfer from the bulk solution to the coolant. The overall heat transfer coefficient for this process is given by

$$\frac{1}{U_{bw}} = \frac{1}{h_w} + \frac{1}{h_i} + \frac{\delta_{wall}}{k_{wall}} \tag{3}$$

where the individual heat transfer coefficients are suitably scaled to have the same heat transfer area.

The energy balance for a small control volume in the coolant flow gives

$$U_{bw}(T_{sb} - T_w)\,dA = -M_w C_{pw}\,dT_w \tag{4}$$

The mass transfer rate equation from the interface to the bulk solution can be expressed as

$$dm_{ws} = K_m \rho_s (\omega_{sb} - \omega_{if})\,dA \tag{5}$$

The liquid–vapor interface condition is obtained by applying the energy equation to an infinitesimally thin control volume enclosing the interface. This gives:

$$dm_{ws} i_v = dm_{ws} i_{pw} + h_o (T_{if} - T_{sb})\,dA \tag{6}$$

where $i_{pw}$ is the partial enthalpy of the absorbed water at the interface, which is a function of the interface temperature and concentration [11].

From Eqs. (5) and (6) the interface condition is obtained as:

$$K_m \rho_s (\omega_{sb} - \omega_{if}) i_{ab}\,dA = h_o (T_{if} - T_{sb})\,dA \tag{7}$$

where $i_{ab} = (i_v - i_{pw})$, is the enthalpy of absorption in the liquid.

For the relatively narrow range of conditions over which practical absorbers operate, the equilibrium condition at the interface at constant pressure can be expressed in the linear form

$$\omega_{if} = a + bT_{if} \tag{8}$$

From Eqs. (7) and (8), the interface concentration may be written in the form

$$\omega_{if} = \frac{\lambda(a + bT_{sb}) + b\omega_{sb}}{(\lambda + b)} \tag{9}$$

where

$$\lambda = \frac{h_o}{i_{ab} K_m \rho_s} \tag{10}$$

Combining Eqs. (1) and (5) and substituting for $\omega_{if}$ from Eq. (9) the solution mass conservation equation takes the form

$$\frac{dM_s}{dA} = K_{ef} \rho_s [\omega_{sb} - (a + bT_{sb})] \tag{11}$$

where the effective mass transfer coefficient is defined as

$$\frac{1}{K_{ef}} = \frac{1}{K_m} + \frac{b i_{ab} \rho_s}{h_o} \tag{12}$$

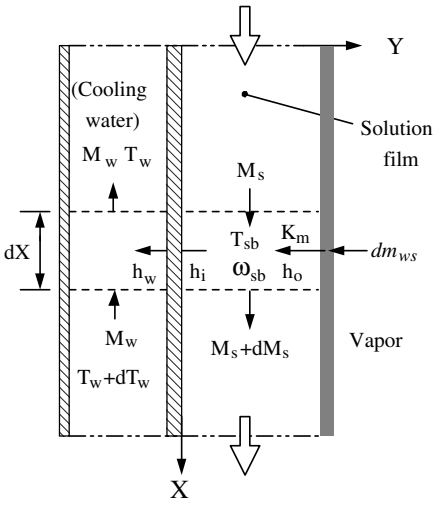


Fig. 1. Physical model.

Combining Eqs. (1) and (2) the energy equation can be expressed in the form

$$M_s \frac{di_s}{dA} = i_{vs} \frac{dM_s}{dA} - U_{bw}(T_{sb} - T_w) \tag{13}$$

where $i_{vs} = i_v - i_s$, is the difference between the vapor and bulk solution enthalpies.

The solution enthalpy $i_s$ is a function of the solution temperature and the concentration. Expressions in polynomial form are available for this dependence from data sources [15]. Using these polynomial expressions, Eq. (13) can be simplified to the form

$$M_s c_s \frac{dT_{sb}}{dA} + M_s c_w \frac{d\omega_{sb}}{dA} = i_{vs} \frac{dM_s}{dA} - U_{bw}(T_{sb} - T_w) \tag{14}$$

The coefficients on the LHS of Eq. (14)

$$c_s = \left[\frac{\partial i_s}{\partial T_{sb}}\right]_{\omega_{sb}} \quad \text{and} \quad c_w = \left[\frac{\partial i_s}{\partial \omega_{sb}}\right]_{T_{sb}} \tag{15}$$

are obtained by differentiating the polynomial expressions.

Since the mass of the absorbent in the solution is constant, the mass flow rate can be written as

$$M_s = \frac{M_l}{\omega_{sb}} \tag{16}$$

Differentiating Eq. (16)

$$\frac{d\omega_{sb}}{dA} = -\left[\frac{M_l}{M_s^2}\right]\left[\frac{dM_s}{dA}\right] \tag{17}$$

Substituting in Eq. (14) from Eqs. (11) and (17)

$$\frac{dT_{sb}}{dA} = K_{ef}\rho_s\left(\frac{i_{vs}}{M_s c_s} + \frac{c_w M_l}{c_s M_s^2}\right)[\omega_{sb} - (a + bT_{sb})] - \left(\frac{U_{bw}}{M_s c_s}\right)(T_{sb} - T_w) \tag{18}$$

Rearranging Eq. (4) the energy equation for the coolant can be expressed as

$$\frac{dT_w}{dA} = -\left(\frac{U_{bw}}{M_w C_{pw}}\right)(T_{sb} - T_w) \tag{19}$$

The set of governing equations to predict the variations of $T_{sb}$, $\omega_{sb}$ and $T_w$ consist of the three first-order non-linear differential Eqs. (11), (17)–(19) and the relations (15) and (16). These equations are solved using the Runge–Kutta method. For the absorbent solution, the temperature and concentration are usually specified at the inlet. In the counter-flow arrangement, that is common in practice, the coolant temperature is known at the outer end of the absorber. Due to the nature of the boundary conditions an iterative procedure where the temperature of the coolant at the outlet is guessed has to be adopted.

### 2.2. Linearized coupled model

Although the simplified model developed in the foregoing section requires much less computational effort than a detailed numerical model, it however does not yield an analytical solution for the governing equations. Fortunately, a careful scrutiny of the magnitudes of the operating parameters of practical absorbers shows that it is possible to make two additional assumptions in the governing equations with little loss of accuracy in the predictions. These assumptions are justifiable because of the relatively small increase in the solution mass flow rate due to vapor absorption [2,3]. With these assumptions the system of governing equations developed above becomes linear and therefore it is feasible to obtain an analytical solution.

Using Eqs. (11), (16) and (17) the mass conservation equation can be written as

$$\left(\frac{M_l}{\omega_{sb}^2}\right)\frac{d\omega_{sb}}{dA} = -K_{ef}\rho_s[\omega_{sb} - (a + bT_{sb})] \tag{20}$$

To linearize Eq. (20) the value of $\omega_{sb}$ in the coefficient of the LHS is replaced with the average concentration between the inlet and outlet

$$\bar{\omega} = \frac{(\omega_{sb,o} + \omega_{sb,ex})}{2} \tag{21}$$

The linearized form of Eq. (20) may be rearranged in the form

$$\frac{d\omega_{sb}}{dA} = -K_{ef}\rho_s\left(\frac{\bar{\omega}^2}{M_l}\right)[\omega_{sb} - (a + bT_{sb})] \tag{22}$$

In order to linearize Eq. (14) the solution mass flow rate is assumed to be constant at the average value

$$\overline{M}_s = \frac{(M_{s,o} + M_{s,ex})}{2} \tag{23}$$

In addition, the coefficients $c_s$ and $c_w$ are assumed to be constant values that are computed by taking the average between the inlet and outlet values.

Subject to the above assumptions, Eqs. (14) and (11) can be combined to give

$$\overline{M}_s\bar{c}_s\frac{dT_{sb}}{dA} + \overline{M}_s\bar{c}_w\frac{d\omega_{sb}}{dA} = i_{vs}K_{ef}\rho_s[\omega_{sb} - (a + bT_{sb})] - U_{bw}(T_{sb} - T_w) \tag{24}$$

From Eqs. (22) and (24) the following equation is obtained

$$\frac{dT_{sb}}{dA} = K_{ef}\rho_s\left(\frac{\bar{c}_w\bar{\omega}^2}{M_l\bar{c}_s} + \frac{i_{vs}}{\overline{M}_s\bar{c}_s}\right)[\omega_{sb} - (a + bT_{sb})] - \left(\frac{U_{bw}}{\overline{M}_s\bar{c}_s}\right)(T_{sb} - T_w) \tag{25}$$

A scrutiny of the governing Eqs. (19), (22) and (25) reveals that by defining two new variables for the temperature difference and the concentration difference, the above equations could be reduced to two coupled linear differential equations. These new variables are defined as:

$$\theta = T_{sb} - T_w \quad \text{and} \quad \psi = \omega_{sb} - (a + bT_{sb}) \tag{26}$$

The temperature difference, $\theta$ between the bulk solution and the coolant is proportional to the heat flux. $\psi$ is the difference between the bulk solution concentration and the equilibrium concentration corresponding to bulk solution temperature, $T_{sb}$. It is seen from (11) that $\psi$ is proportional to the mass flux.

Expressing Eqs. (19), (22) and (25) in terms of the $\theta$ and $\psi$ the following equations are obtained.

$$\frac{d\theta}{dA} = -g_2\theta + g_1\psi \tag{27}$$

$$\frac{d\psi}{dA} = g_3\theta - g_4\psi \tag{28}$$

where the coefficients are given by:

$$g_1 = \left(\frac{K_{ef}\rho_s}{\overline{M}_s\bar{c}_s}\right)\left(\frac{\bar{c}_w\overline{M}_s\bar{\omega}^2}{M_l} + i_{vs}\right) \tag{29}$$

$$g_2 = U_{bw}\left(\frac{1}{\overline{M}_s\bar{c}_s} - \frac{1}{M_wC_{pw}}\right) \tag{30}$$

$$g_3 = \left(\frac{bU_{bw}}{\overline{M}_s\bar{c}_s}\right) \tag{31}$$

$$g_4 = \left(\frac{K_{ef}\rho_s}{\overline{M}_s\bar{c}_s}\right)\left[\frac{\overline{M}_s\bar{c}_w\bar{\omega}^2}{M_l}\left(b + \frac{\bar{c}_s}{\bar{c}_w}\right) + bi_{vs}\right] \tag{32}$$

Variables $g_2$ and $g_3$ occur in traditional exchanger analysis while $g_1$ and $g_4$ are similar variable that includes an effective mass transfer coefficient $K_{ef}$ representing the combined mass and heat transfer process from the interface to the bulk solution. It is seen from Eqs. (27) and (28), that $g_1 = 0$ gives the solution for a counter-flow heat exchanger while $g_3 = 0$ corresponds to an adiabatic mass absorber.

The linear-coupled differential equations (27) and (28) are solved analytically using the Laplace transformation technique. The final forms of the solution are as follows:

$$\theta(A) = a_1e^{\alpha_1 A} + a_2e^{\alpha_2 A} \tag{33}$$

and

$$\psi(A) = b_1e^{\alpha_1 A} + b_2e^{\alpha_2 A} \tag{34}$$

where the roots of the characteristic equation are:

$$\alpha_1, \alpha_2 = -0.5(g_2 + g_4) \pm 0.5[(g_2 + g_4)^2 - 4(g_2g_4 - g_1g_3)]^{1/2} \tag{35}$$

The coefficients are given by:

$$a_1 = \frac{\theta_o(\alpha_1 + g_4) + \psi_o g_1}{\alpha_1 - \alpha_2} \tag{36}$$

$$a_2 = \frac{\theta_o(\alpha_2 + g_4) + \psi_o g_1}{\alpha_2 - \alpha_1} \tag{37}$$

$$b_1 = \frac{\psi_o(\alpha_1 + g_2) + \theta_o g_3}{\alpha_1 - \alpha_2} \tag{38}$$

$$b_2 = \frac{\psi_o(\alpha_2 + g_2) + \theta_o g_3}{\alpha_2 - \alpha_1} \tag{39}$$

where $\theta_o$ and $\psi_o$ are the values at $A = 0$.

The predictions of the linearized model will be compared with the non-linear coupled model and the numerical simulation results to assess its accuracy. The analytical expressions obtained in the linearized model offer a convenient method to extract the heat and mass transfer coefficients from experimental data. These aspects will be considered in the next sections.

### 2.3. Detailed numerical simulation

A detailed numerical model for a laminar falling film over a vertical plate was developed following a procedure similar to that reported by Choudhury et al. [10]. The coolant flow in the present model is in a counter-flow direction. For the sake of brevity the main governing equations of the numerical simulation model are outlined in the Appendix A.

## 3. Experimental details

The test absorber, shown schematically in Fig. 2, consists of a series of 24 horizontal copper tubes of nominal outer diameter 19 mm, wall thickness 1 mm and effective length 160 mm. These are mounted in a vertical plane with the ends of the tubes connected in such a manner that the cooling water flowing through them follows a serpentine flow path. Copper-constantan thermocouples are installed in the water flow by inserting them through the ends of the tubes. The warm water returning from the absorber is first cooled in a heat exchanger and then passed through a temperature-controlled water bath. The flow rate of water is measured with a rotameter whose accuracy is 3.5%.

The test absorber is housed in a cylindrical glass vessel whose length, inside diameter and wall thickness are 1000, 308 and 5 mm respectively. Two brass plates are fixed to the ends of the glass cylinder with metal flanges and gaskets to prevent leakage of air during operation under vacuum conditions.

The solution of lithium bromide and water is contained in the refrigerant evaporator, which is a cylindrical vessel whose length and inner diameter are 450 and

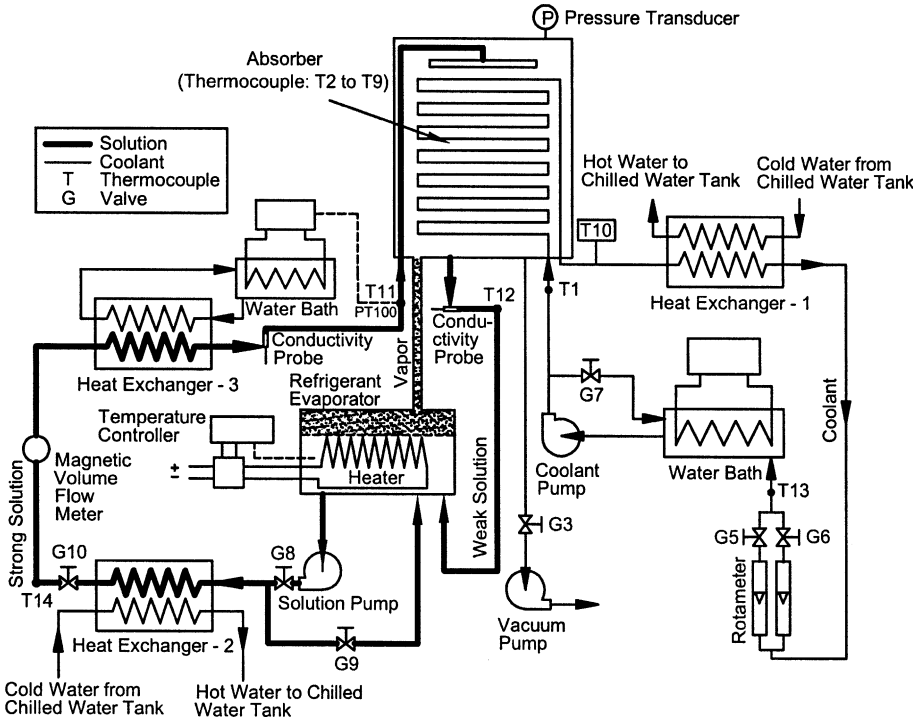


Fig. 2. Schematic diagram of experimental set-up.

325 mm respectively. The water vapor is produced by heating the solution using an electric heater that is controlled to maintain a constant preset temperature in the evaporator. The vapor generated flows through a vertical tube to the absorber vessel located above it.

The solution flow rate is measured with a magnetic flow meter whose accuracy is 1.6%. The solution is sprayed on to the top of the absorber tubes using a solution distributor and absorbs water vapor as it flows as a falling film over the absorber tubes. The weak solution collecting at the bottom of the absorber vessel is returned to the refrigerant evaporator by gravity.

Two conductivity probes are used to measure the concentration of lithium bromide solution at the inlet and exit of the absorber. These are calibrated over a range of mass concentrations and temperatures using samples of lithium bromide of known concentrations before they are installed in the experimental set-up. A series of copper-constantan thermocouples are installed in the solution and cooling water flow circuits. All thermocouples are calibrated using a master thermometer whose uncertainly is 0.05 °C. The output of the thermocouples and the conductivity meters are recorded continuously in a data acquisition system. Additional details on the experimental set-up are available in Raisul Islam et al. [14].

## 4. Analysis of experimental data

The traditional method of obtaining the heat and mass transfer coefficients from experimental data is to use the LMD approach where the heat and mass transfer processes are assumed to be uncoupled. It is apparent from the reported literature that there is no agreement on a consistent definition of the LMDs of temperature and concentration [14]. This leads to wide variations in the reported heat and mass transfer coefficients.

The solutions of Eqs. (27) and (28) provide a consistent and convenient approach to 'extract' the heat and mass transfer coefficients from the present experimental data. Under certain conditions, these solutions also lead to the LMD formulation for heat and mass transfer in the absorber. The analysis of 26 test runs carried out in the present study, showed that the root $\alpha_2$ of Eq. (35) is much larger than $\alpha_1$, typical values being in the ranges $-29$ to $-60$ and $-0.3$ to 0.35 respectively. The analysis of 26 experimental runs for a vertical tube absorber reported by Miller and Keyhani [16], the details of which are also available in Miller [17], showed that the roots $\alpha_2$ and $\alpha_1$ to be in the ranges of $-45$ to $-60$ and 0.35 to 1.1 respectively.

Moreover for both sets of experimental data, the coefficients $a_1$ and $b_1$ are in general larger than $a_2$ and $b_2$ respectively. Due to this the contribution of the term

$e^{\alpha_2 A_t}$ to the values $\theta$ and $\psi$ and at the exit of the absorber can be neglected. However, for calculating the values at the inlet, the contribution of both terms has to be considered.

In view of the above observations, Eq. (28) may be used to develop the following approximate analysis to obtain the LMD based expression for mass transfer. Since

$$|\alpha_2| \gg |\alpha_1| \quad \psi_{ex} = b_1 e^{\alpha_1 A_t} \tag{40}$$

and

$$\psi_o = b_1 + b_2 \tag{41}$$

where $A_t$ is the total area of the absorber.

The total mass absorption rate is obtained by integrating Eq. (11) as

$$\dot{M}_{abs} = K_{ef}\rho_s \int_0^{A_t} [\omega_{sb} - (a + bT_{sb})]\,dA = K_{ef}\rho_s \int_0^{A_t} \psi(A)\,dA \tag{42}$$

Substituting for from Eq. (34) gives

$$\dot{M}_{abs} = K_{ef}\rho_s \left[ \frac{(\psi_{ex} - \psi_o)}{\alpha_1} + b_2 \left( \frac{1}{\alpha_1} - \frac{1}{\alpha_2} \right) \right] \tag{43}$$

From Eqs. (40) and (41) it follows that:

$$\alpha_1 A_t = \ln \left[ \left( \frac{\psi_{ex}}{\psi_o} \right) \left( \frac{b_2}{b_1} + 1 \right) \right] \tag{44}$$

An expression similar to the LMD-form is obtained from Eqs. (43) and (44) as

$$\dot{M}_{abs} = K_{ef}\rho_s A_t \frac{[(\psi_{ex} - \psi_o) + b_2]}{\ln \left[ \left( \frac{\psi_{ex}}{\psi_o} \right) \left( \frac{b_2}{b_1} + 1 \right) \right]} \quad |\alpha_2| \gg |\alpha_1| \tag{45}$$

It is seen that as $b_2 \to 0$ the expression (45) becomes the exact form for the LMD-form for the mass absorption rate.

The corresponding expression for the heat transfer rate may be obtained in a similar manner by using Eq. (33) as

$$Q = U_{bw} A_t \frac{[(\theta_{ex} - \theta_o) + a_2]}{\ln \left[ \left( \frac{\theta_{ex}}{\theta_o} \right) \left( \frac{a_2}{a_1} + 1 \right) \right]} \tag{46}$$

## 5. Results and discussion

### 5.1. Comparison of predictions of models

The predicted temperature and concentration distribution across the film for the absorber with counter-flow cooling water arrangement using the simplified models and the numerical simulation are shown in Figs. 3 and 4 respectively. The convective heat and mass transfer coefficient required in the simplified models have been calculated using expressions (A.14)–(A.16) of the numerical model for the same set of conditions. There is good trend-wise agreement between the predictions of the three models. It is interesting to note that the predictions of the simplified model are slightly lower at shorter distances and becomes slightly higher at longer distance than the prediction of the numerical model. This is presumably due to the use of average heat and mass transfer coefficients in the simplified models.

Figs. 3 and 4 also show that the temperatures and concentrations predicted using the non-linear and linearized coupled models are very close which justifies the simplifying assumptions made to linearize the governing equations. This is encouraging because the analytical solutions of the simplified model offer a convenient means to analyze experimental data and extract heat and

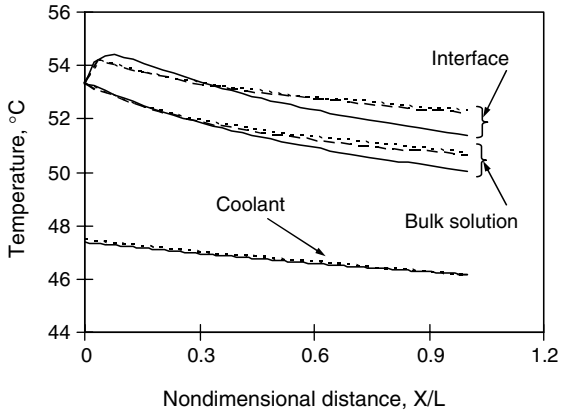


Fig. 3. Temperature distribution for counter-flow absorber. Graphs: (—) numerical model; (– – –) non-linear model; (- - -) linearized mode.

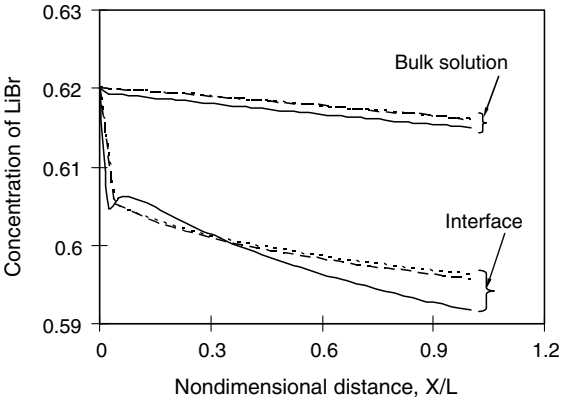


Fig. 4. Concentration distribution for counter-flow absorber. Graphs: (—) numerical model; (– – –) non-linear model; (- - -) linearized mode.

mass transfer coefficients. The above results have demonstrated that with the appropriate average heat and mass transfer coefficients, the simplified models can be used to simulate the performance of lithium bromide-water absorbers.

### 5.2. Determination of heat and mass transfer coefficients

The solutions of the linearized model given by Eqs. (35)–(39) were used to determine the heat and mass transfer coefficients from the present experimental data and the data reported in Miller [17]. The physical model is geometrically similar to the vertical tube absorber used in the latter experiments. The horizontal tubular absorber tested in the present experimental set-up, shown in Fig. 2, on the other hand, had a coolant flow arrangement that could be described as cross-counter to the film flow direction. However, due to the relatively small thickness of the liquid film compared to the tube diameter, the flow configuration may be approximated by a counter-flow cooled vertical falling film.

The values of the variables $\theta$ and $\psi$ at the inlet and outlet of the absorber can be computed directly from the measured temperatures of the solution and the cooling water and the concentrations of the solution using expressions given in Eq. (26). All other parameters such as $\bar{c}_s$, $\bar{c}_w$, $\rho_s$, $a$, $b$ and $i_{vs}$ are obtained from data sources. This leaves $U_{bw}$ and $K_{ef}$ as the only unknowns in Eqs. (33) and (34) which can be determined by solving these equations simultaneously using the Newton–Raphson method [18]. It should be noted that because $h_o$ and $K_m$ are embedded in $K_{ef}$ (Eq. 12) their individual values can only be obtained by invoking an additional condition such as the heat and mass transfer analogy [19].

A comparison between the heat and mass transfer coefficients obtained using the simplified coupled-model and the LMD approach is presented in Figs. 5 and 6 respectively. The LMD quantities are obtained from the exact form of the expressions assuming $b_2 = 0$ in Eq. (45) and $a_2 = 0$ in Eq. (46). The results include data from 26 experimental runs for which the range of conditions and parameters for the model are summarized in Table 1. A detail uncertainty analysis based on the method given Moffat [20] showed the uncertainty of $K_{ef}$ to vary from about 7.5% to 29% while the uncertainty for $U_{bw}$ is in the range from 7.5% to 26%. For some of the data, there is a large difference between the overall heat transfer coefficients, $U_{bw}$ obtained by the two methods. In contrast, the effective mass transfer coefficient, $K_{ef}$ given by the two methods agrees within about 10% for most of the data as seen in Fig. 6. Similar results were obtained for $U_{bw}$ and $K_{ef}$ for the vertical tube absorber studied experimentally by Miller [17].

The heat transfer coefficient $h_i$ from the bulk solution to the tube wall was computed using Eq. (3) where the heat transfer coefficient $h_w$ for the water flow in the tube

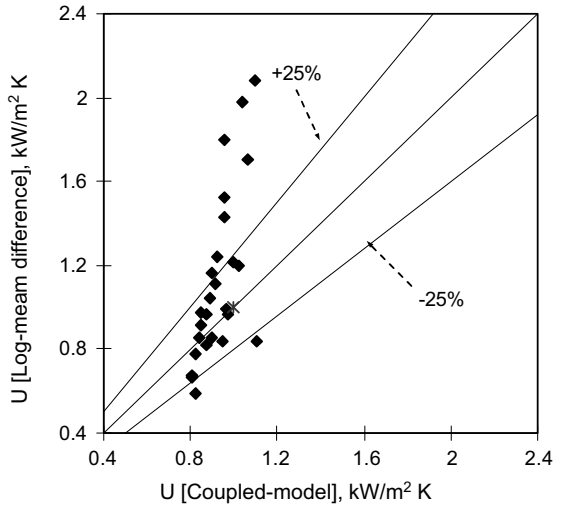


Fig. 5. Comparison of overall heat transfer coefficient using linearized model and LMTD-approach.

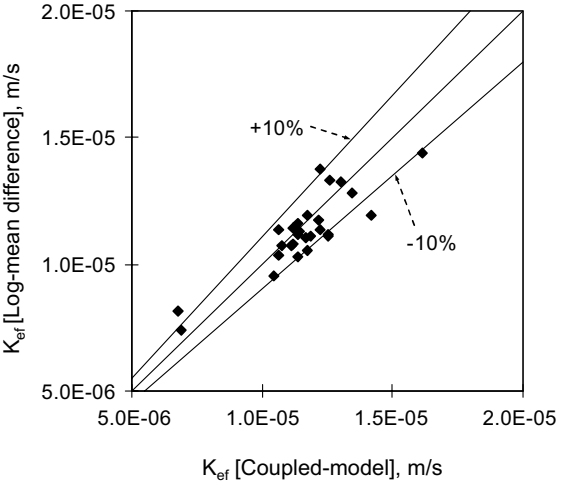


Fig. 6. Comparison of effective mass transfer coefficient using linearized model and LMCD-approach.

was obtained from the Dittus–Boelter correlation [19]. The results are expressed as Nusselt number using Eq. (A.15) and plotted against the film Reynolds number as shown in Fig. 7 for different water inlet temperatures. There is an increasing trend due to the increase in flow rate at higher Reynolds number. The variation of the heat transfer coefficient, $h_i$ is proportional to the ratio of heat flux to the coolant and the temperature difference between the coolant and bulk solution. The increase of the coolant inlet temperature leads to a decrease in the vapor absorption rate. A direct effect of this would be a reduction in the heat flow from the film to coolant.

Table 1
Range of experimental conditions and variables

| Variables | Range |
|---|---|
| $M_{so}$ (kg s$^{-1}$) | $9.5\times10^{-3}$–$1.91\times10^{-2}$ |
| $T_{so}$ (°C) | 39.8–49.7 |
| $\omega_{so}$ | 0.604 |
| $M_w$ (kg s$^{-1}$) | $6.3\times10^{-2}$– $1.14\times10^{-1}$ |
| $T_{wex}$ (°C) | 26–35.5 |
| $i_{vs}$ (kJ kg$^{-1}$) | 2503–2519 |
| $\bar{c}_s$ (kJ kg$^{-1}$ K$^{-1}$) | 1.937–1.969 |
| $\bar{c}_w$ (kJ kg$^{-1}$) | 498.9–547.7 |
| $a$ | 0.274–0.371 |
| $b$ (°C$^{-1}$) | 0.00477–0.00492 |

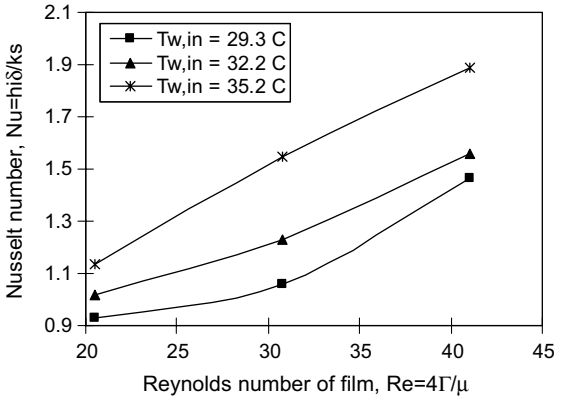


Fig. 7. Variation of Nusselt number with Reynolds number.

However, the higher coolant temperature will also cause the temperature difference between the coolant and the solution to decrease. Fig. 7 shows that the latter, i.e. the decrease in the temperature difference has a more dominant effect, which results in an increase in $h_i$ with coolant temperature. The recent analytical study of Jeong and Garimella [21] has demonstrated that drop formation between tubes could also affect the heat transfer rates significantly at higher flow rates.

The effective mass transfer coefficient $K_{ef}$ was not decomposed into $K_m$ and $h_o$ using Eq. (12) because of the need to assume a form for the heat and mass transfer analogy. It is seen from Eqs. (8)–(10) that the ratio, $h_o/K_m$ can be determined by measuring the film interface temperature [12]. However, since the heat and mass transfer process from the film interface to the bulk solution are coupled, it may be more meaningful to consider $K_{ef}$ as the design variable of interest. It is clear from Eq. (12) that when the fluid properties are assumed to be constant, $K_{ef}$, $K_m$ and $h_o$ are proportional to each other. The mass transfer results are therefore expressed as an effective Sherwood number based on $K_{ef}$ and plotted against the Reynolds number in Fig. 8. There is an increasing trend presumably due to the higher mass absorption resulting from the larger film surface area at higher flow rates. Higher coolant temperatures tend to increase $K_{ef}$ as evident from Fig. 8. The mass absorption and resulting absorption heat generation was found to decrease with increasing cooling water temperature. However, the higher solution bulk temperature resulting from the increased coolant temperature will tend to decrease the temperature and concentration difference between the interface and the bulk solution. The effective mass transfer coefficient, which is proportional to the ratio of the mass flux to the concentration difference, seems to be effected more by the latter with a consequential increase in its magnitude.

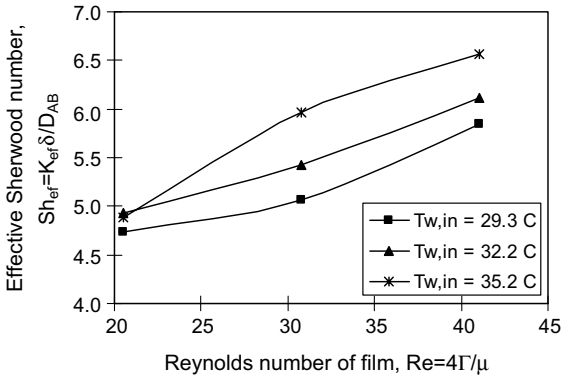


Fig. 8. Variation of effective Sherwood number with Reynolds number.

The temperature distribution of cooling water was calculated by integrating Eq. (19) after substituting for $(T_{sb} - T_w)$ from Eq. (33). The results are shown in Fig. 9

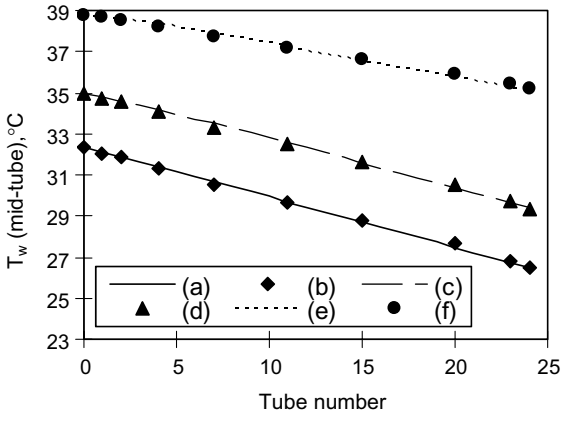


Fig. 9. Variation of cooling water temperature in the direction of solution flow for different flow rates and inlet temperatures of cooling water. Graphs: for $T_{w,in} = 26.5$ °C, $M_w = 0.063177$ kg/s (a) predicted, (b) measured; for $T_{w,in} = 29.3$ °C, $M_w = 0.063177$ kg/s (c) predicted, (d) measured; for $T_{w,in} = 35.2$ °C, $M_w = 0.088759$ kg/s (e) predicted, (f) measured.

for several operating conditions. The good agreement between the prediction and measured temperature lends additional credence to the validity of the coupled-model and to the consistency of the heat and mass transfer coefficients obtained from the model. It is interesting to note that the variation of the water temperature is nearly linear which shows that the heat flux is approximately constant as pointed out by Miller and Keyhani [16].

## 6. Conclusion

The accuracy of a linearlized coupled model for the heat and mass transfer in falling-film absorbers was established by comparing its predictions with a non-linear model and a detailed numerical simulation. Under certain conditions, the linearized model may be reduced to the traditional LMD formulation. The analytical expressions resulting from the linearized model are used to extract the heat and mass transfer coefficients from the experimental data for a horizontal tubular absorber and a vertical tube absorber. The mass transfer coefficients obtained using the linerized model and the LMD formulation agree within about 10% while the heat transfer coefficients showed large differences. The overall Nusselt number and Sherwood number for the tubular absorber increase with increasing film Reynolds number and inlet cooling water temperature. The predictions of the cooling water temperature distribution within the absorber by the linearized model agree well with measurements.

## Acknowledgements

The authors acknowledge with gratitude a grant awarded by the National University of Singapore (RP3981627) under which this work was performed.

## Appendix A. Numerical simulation model

The physical model is shown schematically in Fig. 10. The following assumptions are made in developing the numerical model:

1. The solution is a Newtonian fluid and its physical properties are constant and independent of temperature and pressure.
2. Heat transfer by conduction and mass transfer by diffusion in the direction of solution flow are negligible.
3. Heat transfer in the vapor phase is negligible compared to that in the liquid phase.
4. Vapor pressure equilibrium exists between the vapor and the liquid at the interface.

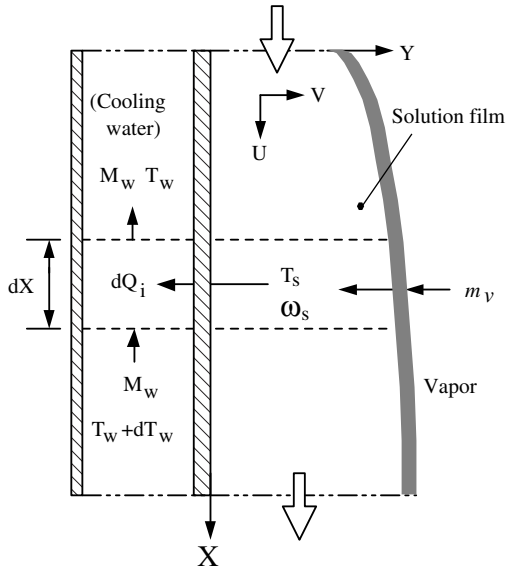


Fig. 10. Physical model for numerical simulation.

5. No shear forces are exerted on the liquid by the vapor.
6. There are no natural convection effects in the film due to temperature or concentration differences.
7. The flow is laminar and non-wavy throughout.
8. The system is in a steady-state.
9. There are no chemical reactions.

*Analysis*

The velocity component of the falling film in the direction of flow is assumed to given by the Nusselt profile [19]

$$U = \frac{g\delta^2}{2v}\left[2\left(\frac{Y}{\delta}\right) - \left(\frac{Y}{\delta}\right)^2\right] \tag{A.1}$$

For constant properties and no velocity gradient along the $Z$-direction, the velocity in the $Y$-direction can be obtained from continuity equation as

$$V = -\frac{gY^2}{2v}\frac{\mathrm{d}\delta}{\mathrm{d}X} \tag{A.2}$$

Film thickness is assumed to have the Nusselt form

$$\delta = \left(\frac{3\Gamma v}{g\rho_s}\right)^{\frac{1}{3}} \tag{A.3}$$

The species transport equation for LiBr with diffusion only in the $Y$-direction and convection due to mass-average motion of the mixture along $X$- and $Y$-directions is

$$\frac{\partial}{\partial X}[U\omega_s] + \frac{\partial}{\partial Y}[V\omega_s] = D_{AB}\frac{\partial}{\partial Y}\left[\frac{\partial \omega_s}{\partial Y}\right] \tag{A.4}$$

Similarly, the energy equation gives

$$\frac{\partial}{\partial X}[UT_s] + \frac{\partial}{\partial Y}[VT_s] = \alpha \frac{\partial}{\partial Y}\left[\frac{\partial T_s}{\partial Y}\right] \tag{A.5}$$

Heat transfer from solution through the absorber wall for the control element (Fig. 10) can be expressed as

$$dQ_i = dA k_s \left.\frac{dT_s}{dY}\right|_{Y=0} \tag{A.6}$$

Heat gained by the cooling water of the control element can be written as

$$dQ_i = -M_w C_{pw} dT_w = dA h_w (T_{wall} - T_w) \tag{A.7}$$

The set of Eqs. (A.1)–(A.7) constitute the governing differential equations that can be expressed in term of the two field variables $T_s$ and $\omega_s$.

The following are the general boundary conditions used in the physical model:

1. At $X = 0$ and $0 \leqslant Y \leqslant \delta$; $T_s = T_{s,o}$, $\omega_s = \omega_{s,o}$ and $\Gamma = \Gamma_o$ (A.8)
2. At $X = L$ and $0 \leqslant Y \leqslant \delta$; $T_w = T_{w,in}$ (A.9)
3. At $0 \leqslant X \leqslant L$ and $Y = 0$; $T_s = T_{wall}$ and $\dfrac{d\omega_s}{dY} = 0$ (A.10)
4. At $0 \leqslant X \leqslant L$ and $Y = \delta$; mass flux of water

$$\dot{m}_v = -\frac{\rho_{s,if} D_{AB}}{\omega_{if}} \left.\frac{d\omega_s}{dY}\right|_{Y=\delta} \tag{A.11}$$

Assuming that the heat of absorption of vapor at the interface is conducted into the film, the energy balance at the interface can be expressed as

$$\dot{q} = \dot{m}_v i_{ab} = k_s \left.\frac{dT_s}{dY}\right|_{Y=\delta} \tag{A.12}$$

where $i_{ab}$ is enthalpy of absorption of vapor in the LiBr solution.

Assuming the equilibrium relationship at the interface to be linear,

$$\omega_{if} = a + bT_{if} \tag{A.13}$$

As the film flows over the plate its thickness increases due to the absorption of water vapor. In order to make the computational domain rectangular, the transformation presented by Choudhury et al. [10], is used. For the sake of brevity, the reader is referred to Ref. [10] for the mathematical details.

The results obtained from the detailed numerical model are used to calculate two heat transfer coefficients $h_o$ and $h_i$ and a mass transfer coefficient $K_m$ for application in the simplified models.

The coefficient of local heat transfer from the film interface to the bulk solution can be expressed through the Nusselt number as

$$Nu_o = \frac{h_o \delta}{k_s} = \frac{\delta}{(T_{if} - T_{sb})} \left.\frac{dT_s}{dY}\right|_{Y=\delta} \tag{A.14}$$

Similarly, the local heat transfer coefficient from the bulk solution to the wall can be written as

$$Nu_i = \frac{h_i \delta}{k_s} = \frac{\delta}{(T_{sb} - T_{wall})} \left.\frac{dT_s}{dY}\right|_{Y=0} \tag{A.15}$$

The mass transfer coefficient from the film interface to the bulk-fluid is defined using Sherwood number as

$$Sh = \frac{K_m \delta}{D_{AB}} = \frac{\dot{m}_v \delta}{D_{AB} \rho_s (\omega_{sb} - \omega_{if})} \tag{A.16}$$

The governing equations have been solved numerically using an upwind scheme with the control volume method. The calculation begins with a guessed value of cooling water outlet temperature. Wall temperature and mass flux of vapor for each row of control volumes are then guessed. Calculation is repeated and guessed values of temperatures and mass fluxes are continuously updated until the guessed and the calculated values are within the specified accuracy. Numerical accuracy for the mass fluxes and temperatures are set at $5 \times 10^{-8}$ kg m$^{-2}$ s$^{-1}$ and $10^{-4}$ °C respectively.

## References


[1] J.D. Killon, S. Garimella, A critical review of models of coupled heat and mass transfer in falling-film absorption, Int. J. Refrig. 24 (2001) 755–797.

[2] V. Patnaik, H. Perez-Blanco, A counter flow heat-exchanger analysis for the design of falling film absorbers, in: International Absorption Heat Pump Conference, AES-31, 1993, pp. 209–216.

[3] V. Patnaik, H. Perez-Blanco, W.A. Ryan, A simple analytical model for the design of vertical tube absorbers, ASHRAE Trans. 99 (2) (1993) 69–80.

[4] A.T. Conlisk, The use of boundary layer techniques in the design of a falling film absorber, in: International Absorption Heat Pump Conference, AES-31, 1993, pp. 163–170.

[5] W.A. Ryan, Water absorption in an adiabatic spray of aqueous lithium bromide solution, in: International Absorption Heat Pump Conference, AES-31, 1993, pp. 155–162.

[6] B.J.C. van der Wekken, R.H. Wassenaar, Simultaneous heat and mass transfer accompanying absorption in laminar flow over a cooled wall, Int. J. Refrig. 11 (1988) 70–77.

[7] T. Bor-Bin, H. Perez-Blanco, Limits of mass transfer enhancement in lithium bromide-water absorbers by active techniques, Int. J. Heat Mass Transfer 41 (1998) 2409–2416.

[8] J.W. Andberg, G.C. Vliet, A simplified model for absorption of vapors into liquid films flowing over cooled horizontal tubes, ASHRAE Trans. 93 (2) (1987) 2454–2466.

[9] H. Uddholm, F. Settewall, Model for dimensioning a falling film absorber in an absorption heat pump, Int. J. Refrig. 11 (1988) 41–45.

[10] S.K. Choudhury, D. Hisajima, T. Ohuchi, A. Nishiguchi, T. Fukushima, S. Sakaguchi, Absorption of vapors into liquid films flowing over cooled horizontal tubes, ASHRAE Trans. 99 (2) (1993) 81–89.
[11] G. Grossman, Simultaneous heat and mass transfer in film absorption under laminar flow, Int. J. Heat Mass Transfer 6 (3) (1983) 357–371.
[12] M.L. Yüksel, E.U. Schlünder, Heat and mass transfer in non-isothermal absorption of gases in falling liquid film. Part I: experimental determination of heat and mass transfer coefficients, Chem. Eng. Process. 22 (1987) 193–202.
[13] M.L. Yüksel, E.U. Schlünder, Heat and mass transfer in non-isothermal absorption of gases in falling liquid film. Part II: theoretical description and numerical calculation of turbulent falling film heat and mass transfer, Chem. Eng. Process. 22 (1987) 203–213.
[14] Md. Raisul Islam, N.E. Wijeysundera, J.C. Ho, Evaluation of heat and mass transfer coefficients for falling-films on tubular absorbers, Int. J. Refrig. 26 (2002) 197–204.
[15] ASHRAE Handbook Fundamentals, American Society of Heating Ventilating and Air-Conditioning Engineers, 1989, pp. 17.69.
[16] W.A. Miller, M. Keyhani, The correlation of simultaneous heat and mass transfer experimental data for aqueous lithium bromide vertical falling film absorption, J. Solar Energy Eng. 123 (2001) 30–42.
[17] W.A. Miller, The experimental analysis of aqueous lithium bromide vertical falling film absorption, PhD thesis, University of Tennessee, Knoxville, 1998.
[18] W.F. Stoecker, Design of Thermal Systems, McGraw-Hill, New York, 1989, pp. 339–346.
[19] D.K. Edwards, V.E. Denny, A.F. Mills, Transfer Processes, McGraw-Hill, New York, 1976.
[20] R.J. Moffat, Describing the uncertainties in experimental results, Exp. Thermal Fluid Sci. 1 (1988) 3–17.
[21] S. Jeong, S. Garimella, Falling-film and droplet mode heat and mass transfer in a horizontal tube LiBr/water absorber, Int. J. Heat Mass Transfer 45 (2002) 1445–1458.